

High 90% efficiency Bragg gratings formed in fused silica by femtosecond Gauss-Bessel laser beams

Mindaugas Mikutis,^{1,2} Tadas Kudrius,^{1,2} Gintas Šlekys,¹
Domas Paipulas,² and Saulius Juodkazis^{3,4}

¹*Altechna RD, Mokslininku st. 6a, LT-08412, Vilnius, Lithuania*

²*Vilnius University, Laser Research Center, Sauletekio Ave. 10, LT-10223 Vilnius, Lithuania*

³*Centre for Micro-Photonics, Faculty of Engineering and Industrial Sciences Swinburne University of Technology, Hawthorn, Vic 3122, Australia*

⁴*The Australian National Fabrication Facility - ANFF, Victoria node, Faculty of Engineering and Industrial Sciences, Swinburne University of Technology, Hawthorn, VIC, 3122, Australia*

mindaugas.mikutis@wophotonics.com

Abstract: Direct laser write of volume Bragg gratings with diffraction efficiency (absolute) $\sim 90\%$ is demonstrated using Gauss-Bessel laser beams in fused silica glass. Axial multiplexing of $\sim 90 \mu\text{m}$ long segments of modified optical material was demonstrated and thick Bragg gratings of aspect ratio $depth/period \approx 234$ were achieved with period $d = 1.5 \mu\text{m}$. Typical fabrication scanning speeds were up to 50 mm/s for gratings with cross sections up to five millimeters made within 1 h time. Potential applications of high efficiency Bragg gratings in a low nonlinearity medium such as silica are discussed.

© 2013 Optical Society of America

OCIS codes: (050.7330) Volume gratings, (140.3390) Laser materials processing, (160.3130) Integrated optics materials, (230.1480) Bragg reflectors.

References and links

1. J. Arns, W. Colburn, and S. Barden, "Volume phase gratings for spectroscopy, ultrafast laser compressors, and wavelength division multiplexing," *Proc. of SPIE* **3779**, 313–323 (1999).
2. O. M. Efimov, L. B. Glebov, and V. I. Smirnov, "High-frequency Bragg gratings in a photothermorefractive glass," *Opt. Lett.* **25**, 1693–1695 (2000).
3. T. Toma, Y. Furuya, W. Watanabe, K. Itoh, J. Nishii, and K. Hayashi, "Estimation of the refractive index change in glass induced by femtosecond laser pulses," *Opt. Rev.* **7**, 14–17 (2000).
4. H. Misawa, S. Juodkazis, S. Matsuo, and T. Kondo, "3D holographic recording method and 3D holographic recording system," US7542186 B2 patent (2009).
5. J. Lumeau and L. B. Glebov, "Modeling of the induced refractive index kinetics in photo-thermo-refractive glass," *Opt. Mater. Express* **3**, 95–104 (2013).
6. C. Voigtländer, D. Richter, J. Thomas, A. Tünnermann, and S. Nolte, "Inscription of high contrast volume bragg gratings in fused silica with femtosecond laser pulses," *Appl. Phys A - Mater. Sci. Process.* **102**, 35 – 38 (2011).
7. K. Yamada, W. Watanabe, K. Kintaka, J. Nishii, and K. Itoh, "Volume grating induced by a self-trapped long filament of femtosecond laser pulses in silica glass," *Jpn. J. Appl. Phys.* **42**, 6916–6919 (2003).
8. K. M. Davis, K. Miura, N. Sugimoto, and K. Hirao, "Writing waveguides in glass with a femtosecond laser," *Opt. Lett.* **21**, 1729–1731 (1996).
9. M. Beresna, M. Gecevičius, and P. Kazansky, "Polarization sensitive elements fabricated by femtosecond laser nanostructuring of glass," *Opt. Mat. Express* **4**, 783 – 795 (2011).
10. M. Malinauskas, A. Žukauskas, G. Bičkauskaitė, R. Gadonas, and S. Juodkazis, "Mechanisms of three-dimensional structuring of photo-polymers by tightly focussed femtosecond laser pulses," *Opt. Express* **18**, 10209–10221 (2010).

11. O. Brzobohatý, T. Čižmár, and P. Zemánek, "High quality quasi-Bessel beam generated by round-tip axicon," *Opt. Express* **16**, 12688–12700 (2008).
12. H. Kogelnik, "Coupled wave theory for thick hologram grating," *Bell Syst. Tech. J.* **48**, 2909–2947 (1969).
13. I. V. Ciapurin, L. B. Glebov, and V. I. Smirnov, "Modeling of phase volume diffractive gratings, part 1: transmitting sinusoidal uniform gratings," *Opt. Eng.* **45**, 015802 (2006).
14. A. Marcinkevicius, V. Mizeikis, S. Juodkazis, S. Matsuo, and H. Misawa, "Effect of refractive index-mismatch on laser microfabrication in silica glass," *Appl. Phys. A* **76**, 257–260 (2003).
15. C. Hnatovsky, R. S. Taylor, P. P. Rajeev, E. Simova, V. R. Bhard-waj, D. M. Rayner, and P. B. Corkum, "Pulse duration dependence of femtosecond-laser-fabricated nanogratings in fused silica," *Appl. Phys.Lett.* **87**, 014104 (2005).
16. S. Richter, M. Heinrich, S. Döring, A. Tünnermann, and S. Nolte, "Formation of femtosecond laser-induced nanogratings at high repetition rates," *Appl. Phys. A* **104**, 503–507 (2011).
17. E. Gaižauskas, E. Vanagas, V. Jarutis, S. Juodkazis, V. Mizeikis, and H. Misawa, "Discrete damage traces from filamentation of Bessel-Gauss pulses," *Opt. Lett.* **31**, 80–82 (2006).
18. A. Marcinkevicius, S. Juodkazis, S. Matsuo, and H. Misawa, "Application of femtosecond non-diffracting bessel beams in micro-structuring of transparent dielectrics," in "Optical Pulse and Beam Propagation III, LASE (Jan. 20–26 2001, San Jose, U.S.A.) SPIE Proc. 4271," (2001), pp. 150–158.
19. S. Juodkazis, V. Mizeikis, S. Matsuo, K. Ueno, and H. Misawa, "Three-dimensional micro- and nano-structuring of materials by tightly focused laser radiation," *Bull. Chem. Soc. Jpn.* **81**, 411–448 (2008).
20. D. Paipulas, V. Kudriasov, K. Kurselis, M. Malinauskas, S. Ost, and V. Sirutkaitis, "Volume bragg grating formation in fused silica with high repetition rate femtosecond Yb:KGW laser pulses," *J. Laser Micro Nanoeng.* **5**, 218–222 (2010).
21. L. Bressel, D. de Ligny, C. Sonnevile, V. Martinez-Andrieux, V. Mizeikis, R. Buividas, and S. Juodkazis, "Femtosecond laser induced density changes in GeO₂ and SiO₂ glasses: fictive temperature effect," *Opt. Mater. Express* **1**, 605–613 (2011).
22. M. Watanabe, S. Juodkazis, H.-B. Sun, S. Matsuo, and H. Misawa, "Luminescence and defect formation by visible and near-infrared irradiation of vitreous silica," *Phys. Rev. B* **60**, 9959–9964 (1999).
23. M. Watanabe, S. Juodkazis, H. Sun, S. Matsuo, and H. Misawa, "Two-photon readout of three-dimensional memory in silica," *Appl. Phys. Lett.* **77**, 13–15 (2000).
24. V. Smirnov, J. Lumeau, S. Mokhov, B. Y. Zeldovich, and L. B. Glebov, "Ultranarrow bandwidth moiré reflecting bragg gratings recorded in photo-thermo-refractive glass," *Opt. Lett.* **35**, 592–594 (2010).
25. R. Buividas, L. Rosa, R. Šliupas, T. Kudrius, G. Šlekys, V. Datsyuk, and S. Juodkazis, "Mechanism of fine ripple formation on surfaces of (semi)transparent materials via a half-wavelength cavity feedback," *Nanotechnology* **22**, 055304 (2011).
26. J. Canning, M. Lancry, K. Cook, A. Weickman, F. Brisset, and B. Poumellec, "Anatomy of a femtosecond laser processed silica waveguide [invited]," *Opt. Mat. Express* **1**, 998–1008 (2012).
27. S. Juodkazis, K. Yamasaki, S. Matsuo, and H. Misawa, "Glass transition-assisted microstructuring in polystyrene," *Appl. Phys. Lett.* **84**, 514 – 516 (2004).
28. C. R. K. Marrian and D. M. Tennant, "Nanofabrication," *J. Vac. Sci. Technol.* **21**, S207–S215 (2003).
29. A. Marcinkevicius, S. Juodkazis, S. Matsuo, V. Mizeikis, and H. Misawa, "Application of Bessel beams for microfabrication of dielectrics by femtosecond laser," *Jpn. J. Appl. Phys.* **40**, L1197–L1199 (2001).
30. M. K. Bhuyan, F. Courvoisier, P. A. Lacourt, M. Jacquot, R. Salut, L. Furfaro, and J. M. Dudley, "High aspect ratio nanochannel machining using single shot femtosecond Bessel beams," *Appl. Phys. Lett.* **97**, 081102 (2010).
31. M. Duocastella and C. B. Arnold, "Bessel and annular beams for materials processing," *Las. Phot. Rev.* **6**, 607–621 (2012).
32. N. Jovanovic, P. G. Tuthill, B. Norris, S. Gross, P. Stewart, N. Charles, S. Lacour, M. Ams, J. S. Lawrence, A. Lehmann, C. Niel, J. G. Robertson, G. D. Marshall, M. Ireland, A. Fuerbach, and M. J. Withford, "Starlight demonstration of the Dragonfly instrument: an integrated photonic pupil-remapping interferometer for high-contrast imaging," *Mon. Not. R. Astron. Soc.* **427**, 806–815 (2012).
33. N. Jovanovic, M. Aslund, A. Fuerbach, S. D. Jackson, G. D. Marshall, and M. J. Withford, "Narrow linewidth, 100 W cw Yb³⁺-doped silica fiber laser with a point-by-point Bragg grating inscribed directly into the active core," *Opt. Lett.* **32**, 2804–2806 (2007).
34. S. Juodkazis, K. Yamasaki, V. Mizeikis, S. Matsuo, and H. Misawa, "Formation of embedded patterns in glasses using femtosecond irradiation," *Appl. Phys. A* **79**, 1549 – 1553 (2004).

1. Introduction

Volume Bragg gratings (VBG) are particular type of phase-gratings embedded in to the volume of transparent material. In comparison with other diffraction gratings, VBG have additional dimension of depth (thickness), that can rise diffraction efficiencies even up to theoretical limit of 100%. Due to this property, VBG are widely used in many photonic applications, mostly in

spectroscopic analysis of weak signals, femtosecond pulse compression, telecommunication [1] and etc. As grating's depth-to-period ratio has to be large, surface relief Bragg gratings are not common. Traditional grating recording technique rely on photosensitivity of the transparent material where interference pattern from UV cw-laser emission [2] or ultrashort laser pulses [3, 4] are recorded directly in the volume of the material. So far hardened gelatin polymer, photo-thermo-refractive and various types of UV-sensitive phosphate glasses were used as a medium for VBG recording [1, 2, 5]. High diffraction efficiencies up to 80% have been demonstrated by VBG in silica recorded through a phase mask [6] and by filamentation tracks [7].

The revelation that it is possible to modify any transparent material with ultrashort laser pulses and to change its refractive index [8], expanded the choice of glasses suitable for VBG recording as a photosensitivity become not required. Fused silica SiO_2 is a good candidate as it is widely used, commercially accessible glass with excellent optical properties. However, to achieve modification in silica a strong focusing into a small focal spot size is required to achieve intensities close to dielectric breakdown for direct laser writing (DLW). This complicates and prolongs recording of large-area/volume structures such as VBG due to the need of axial stitching of modified zones to achieve sufficient depth/period ratio. Filamentation can be utilized for grating inscription [7], however, this process is rather nondeterministic and prevents optimization of essential grating parameters. When dielectric breakdown is used to inscribe photonic structures in glasses and crystals, strong scattering can occur even when features of tens-of-nm are formed at the focus [9]. Thus, it would be very appealing to find a method to write free-form 3D patterns of photomodification of the real part of refractive index, without inducing additional absorption. In sol-gel resist such conditions have been recently demonstrated and 3D structuring without any photo-initiator can be achieved with the highest sub-wavelength resolution [10].

Here we show that highly efficient (with an absolute diffraction efficiency $\sim 90\%$) VBGs can be formed in fused silica without any post-processing or thermal treatment using femtosecond Gauss-Bessel (GB) laser pulses. Axial stitching of focal regions of GB pulses was used to form sub-1 mm traces of optical modification. VBG recorded with GB beams are compared with the gratings formed with Gaussian beams.

2. Experimental

Direct laser writing of VBG was carried out with second harmonic (515 nm) of Yb:KGW laser ("Pharos", Light Conversion Ltd.) having a pulse duration of 170 fs (FWHM) and pulse repetition rate of 200 kHz. Fused silica axicones (apex angles of 179° and 178°) were used to transform Gaussian into a GB beam. A near-IR transmitting microscope objective (Mitutoyo Plan Apo NIR 50 \times) with numerical aperture $NA = 0.42$ was used in conjunction with plano-convex focusing lens to form a demagnifying telescope that decreased the initial size of GB beam by 75 times. Resulted GB beam was imaged inside the sample. Fused silica glass sample (Lithosil, Schott) with refraction index of 1.46, was mounted on high-precision 3D positioning stages (Aerotech) and translated with respect to the GB beam. A VBG recording sequence was fully automated (software SCA, Workshop of Photonics). Schematic representation of the experiment is shown in Fig. 1.

An important feature of the fabrication algorithm was a precise synchronization of the stage movement and beam shutter to help achieve constant spatial overlap of pulses during sample translation. This was achieved by timing the opening and closing of the shutter during acceleration and deceleration periods of the tables. This allowed formation of all gratings with constant exposure conditions. Stage traveling speeds were in range from 1 to 160 mm/s. However, the recording was aimed at the maximum speed which was optimized for stage acceleration, deceleration and grating dimensions.

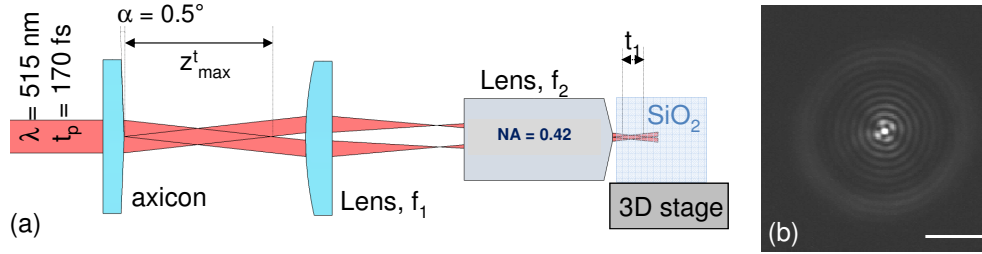


Fig. 1. (a) Schematics of experimental setup for GB beam generation and its downsizing by a telescope. Plano-convex lens with focal length f_1 is used together with $NA = 0.42$ objective lens of a focal length f_2 to produce a conjugated image of GB beam inside the volume of fused silica sample ($f_2/f_1 \simeq t_1/z_{max}^t = 1/75$). (b) Image of the GB beam in the z_{max}^t region (at the edge of the region) produced with an axicon having the 179° apex angle. Scale bar is $5 \mu\text{m}$.

For comparison, VBGs were also recorded with Gaussian beams, by focusing laser radiation directly into the volume of the sample with the same $NA = 0.42$ objective. In this setup we used a fundamental laser radiation wavelength $\lambda = 1030 \text{ nm}$. The spot size $2w_0$ and axial extent $2z_R$ of the Gaussian beam are defined by $2w_0 = \frac{4\lambda f}{\pi D} M^2$ and $2z_R = \frac{\pi w_0^2}{2\lambda}$, where $M^2 = 1.2$ is the quality factor of the used laser beam, D denotes the beam diameter (3.2 mm at $1/e^2$ level) and f stands for the focal length of the objective. Here w_0 and z_R are beam waist radius and Rayleigh length, respectively. For used objective the focal spot was $2w_0 = 1.7 \mu\text{m}$ and $2z_R = 4.5 \mu\text{m}$, respectively.

The GB pulse can be described by its central core diameter ρ_0 , and the axial extent of the "non-diffracting" zone z_{max}^t . These parameters are expressed by the following formulas [11]:

$$\rho_0 = \frac{1.2024\lambda}{\pi \sin(\alpha_0)}, \quad (1)$$

$$z_{max}^t = \frac{w_0 \cos(\alpha_0)}{\sin(\alpha_0)}, \quad (2)$$

where $\alpha_0 = \alpha(n_{ax} - n_0)/n_0$ with n_0 and n_{ax} being refractive indexes of the ambient and axicon, respectively; and α is axicon's half-angle measured in respect of its base (in our case 0.5° for the 179° -apex cone axicon). One would find that for ideal $1/75$ demagnification $\rho_0 = 0.66 \mu\text{m}$ and $z_{max}^t = 116 \mu\text{m}$ (Fig. 1). As can be seen, the axial extent of GB beam is by an order larger than that of the Gaussian beam while the waist diameter remains almost the same. It is noteworthy that the Eqs. (1) and (2) are valid only for an ideal axicon. For DLW, the relevant parameter was the demagnified track length t_1 or the length of non-diffracting zone z_{max}^t in silica.

3. Diffraction properties of VBG

Diffraction properties of the VBG's are analyzed by the coupled wave model devised by H. Kogelnik [12]. According to the model, VBG can reach the highest efficiency operating only at the Bragg diffraction conditions, that can be expressed as:

$$m\lambda/n = 2d \sin(\theta_B); \quad (3)$$

where θ_B is the Bragg angle, d is the period of the grating, λ is the wavelength of diffracted beam, and n is the refractive index of material where diffraction takes place (Fig. 2). It is easy

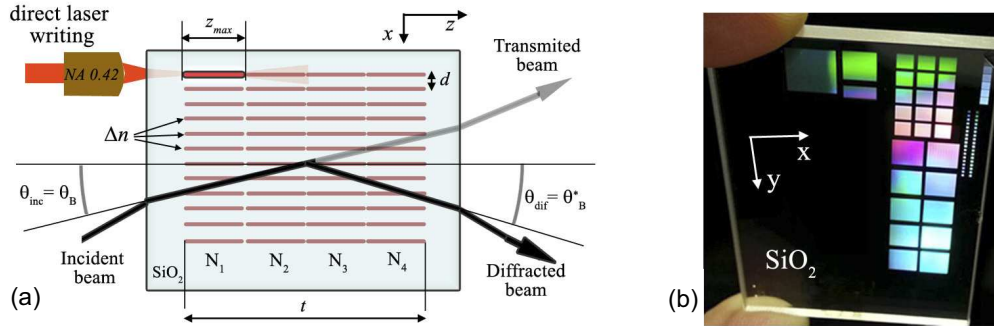


Fig. 2. (a) Schematics of the VBG recorded with GB laser beam. Several layers (N_1 to N_n) of z_{max} depth gratings are stitched together to form one thick grating with overall thickness t . Grating period is d and diffraction is caused by a homogeneous modulation of the refractive index Δn , induced by femtosecond laser pulses. When incident beam satisfies the Bragg condition ($\theta_{inc} = \theta_B = |\theta_{dif}| = |\theta_B^*$), diffraction efficiencies up to 100% could be achieved. (b) Optical images of fused silica sample with VBGs formed by Gaussian and Gauss-Bessel (GB) ultra short laser pulses at different energies, scanning velocities, and having different grating depths.

to see, that Bragg condition can be derived from a classical diffraction equation implying that incident and diffracted beam angles have the same absolute values. For a particular grating and single wavelength there exist several Bragg angles connected through the integer m in Eq. (3); however, the condition that incident and diffracted beam angles have to be the same can be satisfied only once, thus energy interchange takes place only between two beams: diffracted and undiffracted (no higher diffraction orders are analyzed in the coupled wave model).

Diffraction efficiency, defined as the ratio between diffracted and incident beam powers, can be expressed by the following formula:

$$\eta = \sin^2 \left[\frac{\pi \Delta n t}{\lambda \cos(\theta_B)} \right], \quad (4)$$

here Δn is a magnitude of homogeneously modulated refractive index, t is the grating axial extent (thickness). It is easy to see that the product $\Delta n \times t$ determines the VBG efficiency for the single wavelength at Bragg condition. As laser-induced variations of Δn in a non-photosensitive material is somehow limited, the grating depth can be easily changed using a multiplexing procedure: stitching several layers of gratings on top of each other by DLW technique.

Though VBG are designed to operate exactly at the Bragg condition (at the exact wavelength and angle), it is common to define VBG's spectral and angular bandwidth. Expressions defining diffraction efficiencies when grating is detuned from the Bragg angle ($\Delta\theta_i$) or wavelength ($\Delta\lambda$) are the following [13]:

$$\eta(\Delta\theta_i) = \frac{\sin^2 \left[\pi t \sqrt{\Delta n^2 / (\lambda_0 \cos(\theta_B))^2 + (d \Delta\theta_i)^2} \right]}{1 + (\lambda_0 \cos(\theta_B) \Delta\theta_i / d \Delta n)^2}, \quad (5)$$

$$\eta(\Delta\lambda) = \frac{\sin^2 \left[\pi t \sqrt{(\Delta n / \lambda_0)^2 + (d^{-2} \Delta\lambda / 2n)^2} / \cos \theta_B \right]}{1 + (d^{-2} \lambda_0 \Delta\lambda / 2n \Delta n)^2}, \quad (6)$$

here $\Delta\theta_i$ is the small change in angle (as compared to θ_B) expressed in radians. It is important to stress that these formulas are only valid for non-slanted gratings (for complete expressions see

in Ref. [13]). Using these equations it is possible to define the spectral and angular bandwidth, defined as Half Width at First Zero (HWFZ):

$$\Delta\theta_i^{HWFZ} = \frac{\sqrt{3}d}{2t} \sqrt{\frac{4n^2 - \lambda_0^2 d^{-2}}{4 - \lambda_0^2 d^{-2}}}; \quad \Delta\lambda_0^{HWFZ} = \frac{\sqrt{3}nd^2 \cos(\theta_B)}{t}. \quad (7)$$

As can be seen from these expressions, both bandwidths are inversely proportional to the grating thickness (t).

Diffraction efficiencies of all VBG's demonstrated in this work were measured using HeNe laser at 633 nm wavelength at the Bragg condition. We estimated the efficiency by measuring the total power of diffracted beam and compared it to the beam that freely passes through the sample when grating is moved out of the beams path. In such configuration the *absolute* efficiency was evaluated and the glass absorption and Fresnel reflection losses were eliminated by definition. In order to evaluate the spectral bandwidth, a white light continuum (WLC) was shone on the VBGs and spectrum of transmitted (undiffracted) beam was measured in order to evaluate which spectral components were diffracted, hence absent from the WLC spectrum. The WLC was generated in a 2-mm-thick sapphire plate using 1.6 μ J laser pulses at 25 kHz repetition rate (at 1030 nm wavelength with 280 fs duration) and focused with a $NA = 0.03$ lens. Later, a 50 mm focal length lens was used for collimation of the WLC onto VBG.

The samples of VBG formed in fused silica are shown in Fig. 2(b). Smaller dimension gratings at the top right corner ($1 \times 1 \text{ mm}^2$ and smaller) were recorded with pure Gaussian beam, while the larger ($2 \times 2 \text{ mm}^2$, $4 \times 4 \text{ mm}^2$ and $6 \times 6 \text{ mm}^2$) VBGs were formed with GB laser beam. Sufficient thickness of all gratings was achieved by axial multiplexing of the optical modification tracks.

4. Results and discussion

4.1. Structural modifications of silica

Axial modification tracks left by the GB laser beam in fused silica are shown in Fig. 3(a). It is possible to evaluate a modified track length after a single GB shot, which was $88 \pm 5 \mu\text{m}$ for the axicon apex angle of 179° . This value is slightly lower as expected due to existence of a silica modification threshold, but comparable to the one estimated with Eq. (2). In order to stitch several modified tracks, sample has to be moved by z_{max}/n in respect to the previous track. With high precision traveling stages this procedure is straightforward and it was possible to achieve a stitching accuracy down to $\pm 3 \mu\text{m}$. It is noteworthy, such a high precision was achieved since the spherical aberration, unavoidable for focusing of a Gaussian beam through the air-silica boundary [14], is minimized due to the same front tilt of all rings of the GB beam at the interface and each grating layer was comparable in length even after $N = 5$ multiplexing steps. Despite close packing of modified tracks each one is identical to the other (Fig 3(a) tracks are separated by $2.5 \mu\text{m}$, but working gratings with period $d = 1 \mu\text{m}$ were also achieved). Such close packing of tracks also shows that material modification is too weak to induce some observable changes in GB beam propagation by neighboring tracks.

Figure 3(a) shows that material modification in each modified track is not homogeneous: there is a prominent dark central region surrounded by bright zones at the both sides along the track. Bright regions are the areas where material refractive index is increased (so called type-I modification), where the dark regions are due to the formation of scattering centers in fused silica (the type-II modifications). Indeed, these two types of laser-induced modifications are well known to exist in fused silica and depend on the laser pulse intensity [15]. By looking at

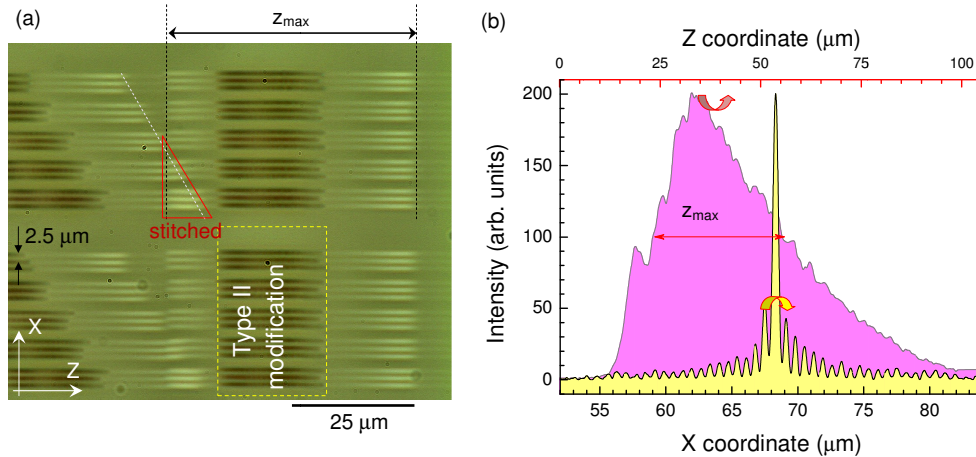


Fig. 3. (a) An optical side-view image of modifications induced with the GB beam and their axial stitching. Central part of the GB trace has intensity above the threshold appearance of type-II modifications causing the scattering centers in fused silica (box enclosure). (b) Axial and lateral intensity cross sections of the GB beam measured after demagnifying telescope in air. The GB in (a) and (b) were generated using an axicon with a 178° apex angle.

the measured axial energy distribution of GB beam (Fig. 3(b)) it is clear that central part has twice as large intensity as compared with slopes, thus explaining the occurrence of two different types of modification. It is important to reduce laser intensity down to the levels where only the type-I modification is dominant. This was achieved by decreasing laser pulse to $1 \mu\text{J}$. The type-II modification appears when laser energy is above $1.8 \mu\text{J}$ (for a single shot) or $1.2 \mu\text{J}$ (for a multi-pulse irradiation). In the single shot case, induced type-II modifications do not exhibit a form-birefringence characteristic to this type of modification. The birefringence caused by formation of regularly orientated nanogratings, develops only after a multi-pulse irradiation. Such modification behavior is well known and was reported earlier [16].

Filamentation of GB beam should be avoided during recording as it is known to produce bead-like damage tracks along pulse propagation path [17]. The typical total pulse power was $P_p = E_p/t_p \simeq 1 [\mu\text{J}]/170 [\text{fs}] = 5.9 \text{ MW}$. Number of rings in GB beam can be evaluated by $N_r = D \sin(\gamma)/\lambda$ [18], where γ is the angle of plane waves with the optical axis which can be found from $\sin(\alpha + \gamma) = n_{ax} \sin(\alpha)$. In our experiment $N_r \simeq 20$. Then, the power per ring is $P_p/N_r \simeq 295 \text{ kW}$ which is lower than the threshold of self-focusing for the Gaussian beam which is $\sim 1 \text{ MW}$ in fused silica [19].

4.2. Characterization of volume Bragg gratings

Experimentally measured diffraction efficiency vs grating thickness is shown in Fig. 4. This plot is useful not only for the estimation of correct VBG grating thickness, but also for the evaluation of laser-induced refractive index modulation level, Δn , which is only unknown parameter in VBG efficiency formula (Eq. (4)), as grating depth can be directly measured using optical microscope [20]. By fitting the scaled efficiency formula to the experimental data $\eta_{exp} = A\eta$, it is possible to evaluate Δn , here A is a scaling factor. A qualitatively good theoretical fit was achieved with $A \simeq 0.91$ and $\Delta n = 9.5 \times 10^{-4}$ for VBG's recorded with $1 \mu\text{J}$ laser pulses. Such

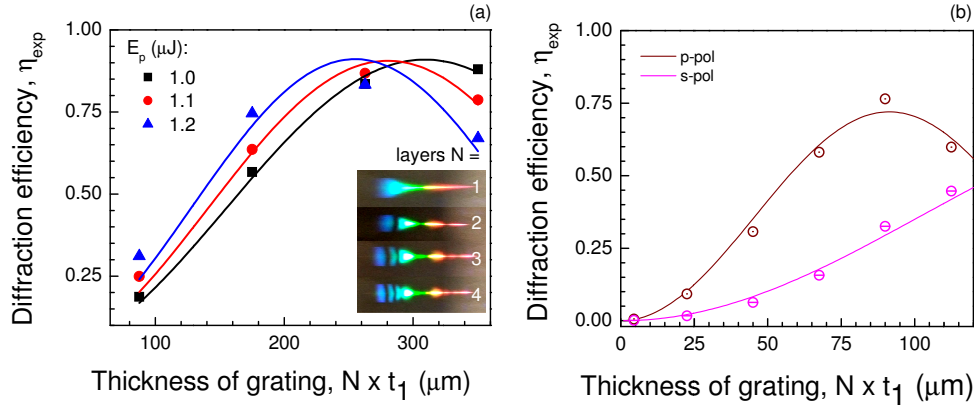


Fig. 4. (a) Diffraction efficiency vs grating thickness for GB beam written VBG. Incident wavelength was 633 nm at the Bragg condition ($\theta_B = 8.3^\circ$) and grating period of 1.5 μm . Thickness was varied by changing multiplexing number from N_1 to N_4 . Single layer had ($t_1 = 88 \mu\text{m}$ thickness. Solid lines are theoretical curves calculated by $\eta_{exp} = A\eta$ (Eq. (4)), where $A \approx 0.91$. Gratings recorded with higher pulse energies have maximum efficiency peak shifted to the left due to increased variation in refractive index Δn . Inset shows images of diffracted WLC light at the same incident angle 8.3° from gratings with different number of multiplexed layers. (b) Diffraction efficiency vs grating thickness for VBG made with a Gaussian beam. Grating period was 2 μm , and single layer axial length $t_1 = 4.5 \mu\text{m}$. Pulse energy was 200 nJ, sample translation speed of 2 mm/s at 200 kHz repetition rate, focusing by $NA = 0.42$ objective. Diffraction depends on polarization s and p of the incident beam due to strong birefringence at the modified zones. Solid lines represents theoretical curves with parameters $A \approx 0.72$, $\Delta n_s = 0.0013$, $\Delta n_p = 0.0029$.

refractive index increase is usual in fused silica due to fast thermal quenching following a local absorption, heating and densification of the glass at high temperatures; the most dense silica is at 1500°C [21]. If laser pulse energy is increased by 20%, Δn increases up to 1.2×10^{-3} according to the efficiency measurements.

Scaling factor A accounts for all factors that causes imperfections of VBG, mainly the anharmonicity of the refractive index modulation, induced scattering and absorption in the laser-modified material. It is known that optical induced defects can be annealed, however, it can influence the magnitude of Δn [22, 23] and it was not attempted in this first study.

We utilized a WLC to characterize performance of VBG as shown in the inset on Fig. 4(a). The spectrum has prominent dark stripes revealing that some wavelengths were not diffracting. This effect can be explained by presence of non-homogeneous axial modifications induced by the GB beam along the depth of the VBG tracks. When several layers are stitched together, a secondary variation of Δn occurs. It is predicted by the coupled wave theory, that if diffracted beam undergoes an additional phase change of π somewhere in the grating, the energy transfer reverses and diffracted beam starts to couple to the un-diffracted one until depletion is reached. This effect is extensively used in Moiré-Bragg gratings [24]. We put conjecture that dark regions reveals spectral locations where π -shifts occurred. The number of lines increased with number of layers. Since VBGs are designed for operation at the narrow spectrum and particular angle, the dark lines can be easily avoided. Improved stitching fabrication is expected to reduce this unwanted effect and will be addressed in future experiments.

Spectral and angular bandwidths of the grating can be measured from WLC spectrum of

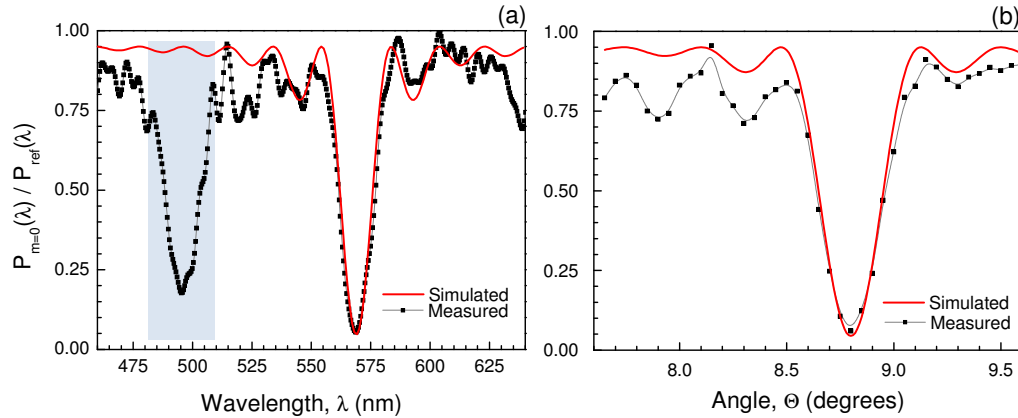


Fig. 5. (a) Spectral sensitivity of the VBG fixed at the 8.8° incidence angle. (b) Angular sensitivity of the grating fixed at the 569 nm wavelength. The data were collected from a normalized WLC spectrum of an undiffracted beam; thus y-scale is inverted. Solid lines represent theoretical simulation according to Eq. (5) and Eq. (6), with model parameters: $t = 352 \mu\text{m}$, $\Delta n = 0.001$, $d = 1.5 \mu\text{m}$. Additional peaks, with their side lobes are due to quality of stitching between regions recorded at different depths as well as axial modulation of refractive index (shaded region in (a)).

un-diffracted beam. These results are shown in Fig 5. Theoretical models described by Eqs. (5) and (6) agree very well with the measured data. For a VBG which is $352 \mu\text{m}$ -thick (or 4 layers of axially multiplexed gratings) and has a period of $1.5 \mu\text{m}$, at a 570 nm wavelength, one can estimate the angular and spectral selectivity to be $\Delta\theta_i^{HWFZ} = 0.31^\circ$ and $\Delta\lambda_0^{HWFZ} = 13.2 \text{ nm}$, respectively according to Eq. (7).

An additional peak not predicted by the Bragg diffraction model is recognizable in Fig. 5(a). This peak could be a grating artifact, arising from minor layer stitching deviations in the transfer x -direction. Indeed, a small shift of $\Delta x \simeq 0.7 \mu\text{m}$ can be seen between all stitched lines in Fig. 3. The origin of this shift is a minute inclination angle of the GB beam in respect to the normal to the silica substrate. It also demonstrates a possibility to inscribe slanted gratings (not considered here).

Gratings made with Gaussian laser beam also show relatively high diffraction efficiencies (Fig. 4(b)), however, a stronger focusing leads to the formation of only type-II modifications that have intrinsic birefringence. Thus, the diffraction efficiency becomes polarization-dependant. The VBGs made from type-II modifications can have smaller depths as the induced refractive index variation is three times larger as compared to the GB case. However, this does not help to reduce fabrication time as smaller axial length of modification requires higher level of multiplexing $N > 20$. A sample translation speed has to be low in order to achieve type-II modification with minimal scattering [20] which prolongs recording even further and makes it impractical.

The highest achieved diffraction efficiency recorded with GB beam achieved was 89% at 633 nm wavelength and is among the best demonstrated in silica [6, 7]. A VBG depth was $352 \mu\text{m}$ (formed by 4 layers) and period was $1.5 \mu\text{m}$, hence the grating aspect ratio $depth/period = 234$. Its lateral size was $6 \times 6 \text{ mm}^2$, which took less than an hour to record with ultra-short GB laser pulses. No thermal post-processing was applied. This shows potential to reach very high diffraction efficiency in pure silica by direct laser writing. Interestingly, the

efficiency of the Bragg grating was same for the s - and p -polarizations. This indicates that there was no nano-ripples formed at the laser affected regions which is typical for the laser induced damages by focused Gaussian beam [15]. It can be shown that at the near-breakdown conditions a strong ionization occurs via nano-sphere to nano-plane formation which can be simulated by electrostatic approximation [25] and causes the formation of nano-gratings responsible for the form birefringence. The photo-modified GB traces in silica with augmented refractive index can be nano-porous and at the same time denser [26], hence, not exerting stress on the neighboring regions. This explains the absence of birefringence due to stress and/or form-birefringence in our case. The smallest period gratings recorded by axial multiplexing of $N = 5$ layers with GB beams was $1 \mu\text{m}$.

5. Conclusion and outlook

Diffraction Bragg gratings with efficiency $\sim 90\%$ have been demonstrated by direct laser writing with GB laser pulses. Axial multiplexing of up to $N = 4$ layers was necessary to maximize diffraction efficiency. Strongly dispersive gratings with period of $1.5 \mu\text{m}$ were successfully recorded within 1 h time span over the footprint areas $6 \times 6 \text{ mm}^2$. Stitching of gratings axially by the direct write approach demonstrated here proves to be more efficient as compared with a write-and-stretch approach attempted in polymers [27]. Fabrication of a fully functional optical device performing at a high $\sim 90\%$ efficiency inside $6 \times 6 \times 0.35 \text{ mm}^3$ volume within 1 hour shows the state-of-the-art of fs-DLW. It performs at industrial requirements for the nanofabrication throughput, T , predicted by the Tennant's law [28], which for planar-2D lithography based procedures $R = 2.3 \times T^{0.2}$; here T is in $[\mu\text{m}^2/\text{hour}]$ at resolution, R [nm]. If rescaled for the 3D nanofabrication case considering the same scaling, one can project $R = 2.3 \times T_{3D}^{0.3}$ where T_{3D} $[\mu\text{m}^3/\text{h}]$. The resolution of fabricated VBG $R \sim 1 \mu\text{m}$ and the throughput of $T_{3D} \sim 10^9 \mu\text{m}^3/\text{h}$ are closely following the Tennant's prediction for an industrial application.

Femtosecond GB beams can be used for recording extended traces of optical damage inside transparent dielectrics [29], can ablate tens-of-micrometers long channels of only few microns in diameter in glass in a single shot [30] and has increasing range of applications beyond laser fabrication as discussed in recent review [31]. VBGs of high diffraction efficiency recorded over large areas can find applications as spectral and angular filters together with optical lanterns used for pupil-remapping in astro-physical applications [32]. Among other applications where fs-DLW with GB beams can be used are high-power lasers directly written in active glasses [33] and wet etching of laser fabricated patterns [34].

Acknowledgments

This work was supported by research grant No. VP1-3.1-SMM-10-V-02-007 – Development and utilization of a new generation industrial laser material processing using ultrashort pulse lasers for industrial applications – from the European Social Fund Agency. SJ is grateful for support via Australian Research Council Discovery DP120102980 grant.